Supporting Information for:

An Ultra-Stable Nonheme Oxoiron(IV) Complex and Its Blue Conjugate Base.

Jason England,[a] Jennifer O. Bigelow[a], Katherine M. Van Heuvelen[a], Erik R. Farquhar[a], Marléne Martinho[b], Katlyn K. Meier[b], Jonathan R. Frisch[a], Eckard Münck*[b], and Lawrence Que, Jr.*[a]

Contents:

Experimental

General Considerations

All reagents were purchased from Aldrich and used as received, unless noted otherwise. Diethyl ether and tetrahydrofuran (THF) were dried by prolonged reflux, under a nitrogen atmosphere, over sodium metal with a benzophenone ketyl indicator and distilled freshly prior to use. Acetonitrile was treated in a similar manner, but using calcium hydride as the drying agent. Isonitrile impurities in butyronitrile were removed by washing with concentrated hydrochloric acid. Subsequent rapid stirring over powdered anhydrous potassium carbonate served to neutralize acidic impurities and absorb water. After further drying over calcium hydride, the purified solvent was distilled under a nitrogen atmosphere and degassed prior to use. Iodosobenzene,[1] $Fe(OTf)_2(CH_3CN)_2$,[2] 1,4,8-Me_3cyclam-11-$CH_2C(O)NMe_2$,[3] and 0.2 M toluene solution of tetraoctylammonium hydroxide ($NOct_4OH$)[4] were all prepared according to published procedures. All moisture- and oxygen-sensitive compounds were prepared using standard high vacuum line, Schlenk, or cannula techniques. A standard nitrogen-filled glove box was used for any subsequent manipulation and storage of these compounds. Elemental analyses were performed by Atlantic Microlab (Norcross, GA).

Preparation of Complexes

[Fe^{II}(1,4,8-Me_3cyclam-11-$CH_2C(O)NMe_2$)](OTf)$_2$ (**4**): A mixture of 1,4,8-Me_3cyclam-11-$CH_2C(O)NMe_2$ (0.34 g, 1.04 mmol), $Fe(OTf)_2(CH_3CN)_2$ (0.46 g, 1.04 mmol) and THF (10 mL) were stirred together overnight. The pale green precipitate that formed during this time was isolated by filtration, washed with THF (2 × 5 mL) and diethyl ether (20 mL), and dried under vacuum to give the product as a cream-colored solid (0.49 g, 69%). Crystals suitable for X-ray analysis were grown by vapor diffusion of diethyl ether into a concentrated acetonitrile solution of complex. ^{1}H-NMR (CD_3CN, 293 K, all peaks appear as broad singlets): δ 390.0 (1H, CH_2), 376.5 (1H, CH_2), 338.8 (1H, CH_2), 314.7 (1H, CH_2), 251.2 (1H, CH_2), 207.6 (1H, CH_2), 195.6 (1H, CH_2), 171.1 (1H, CH_2), 168.4 (1H, CH_2), 108.4 (3H, N*Me*), 105.5 (1H, CH_2), 103.6 (3H, N*Me*), 98.5 (4H, N*Me* + CH_2), 101.9 (1H, CH_2), 79.9 (1H, CH_2), 50.5 (3H, C(O)N*Me*), 34.8 (1H, CH_2), 17.3 (1H, CH_2), 12.4 (4H, C(O)N*Me* + CH_2), 7.5 (1H, CH_2), -4.0 (1H, CH_2), -16.9 (1H, CH_2), -34.5 (1H, CH_2), -36.8 (1H, CH_2), -97.3 (1H, CH_2). MS (+ESI): *m/z* 532.1 [(M-OTf)$^+$]. Anal. Calcd. (found) for $C_{19}H_{37}F_6FeN_5O_7S_2$: C, 33.49 (33.51); H, 5.47 (5.52); N, 10.28 (10.11).

[Fe^{IV}(O)(1,4,8-Me_3cyclam-11-$CH_2C(O)NMe_2$)](OTf)$_2$ (**5**): Excess PhIO (approx. 3 equiv) was added to acetonitrile/butyronitrile solutions of **4** and the resultant mixtures stirred together at room temperature for 15 minutes. Subsequent removal of excess oxidant by filtration provided pale brown solutions of **5** suitable for kinetic and spectroscopic studies. Crystals suitable for X-ray analysis were grown at -35 °C, by layering concentrated (> 10 mM) acetonitrile solutions of 5 with diethyl ether. ^{1}H-NMR of 5 (CD_3CN, 233 K, all peaks appear as broad singlets): δ 94.1 (1H, NCH_2), 86.6 (1H, NCH_2), 62.5 (1H, CCH_2C), 53.6 (1H, CCH_2C), 36.5 (2H, CCH_2C + NCH_2), 34.0 (2H, CCH_2C + NCH_2), 23.3 (3H, C(O)N*Me*), 20.7 (1H, NCH_2), 15.1 (4H, C(O)N*Me* + NCH_2), -5.3 (1H, NCH_2), -40.0 (1H, NCH_2), -52.2 (1H, NCH_2), -57.6 (6H, 2 × N*Me*), -64.3 (3H, N*Me*), -81.0 (1H, NCH_2), -138.4 (2H, NCH_2), -201.3 (1H, NCH_2), -206.9 (1H,

NC*H*$_2$), -211.9 (2H, NC*H*$_2$).

[Fe^{IV}(O)(1,4,8-Me$_3$cyclam-11-CH=C(O)NMe$_2$)](OTf) (**6**): Addition of 5 equiv of NBu$_4$OH (available commercially as a hydrate with 30 molecules of water) to acetonitrile solutions of **5** yielded blue solutions of **6** that were relatively stable at -40 °C, but decayed readily at 25 °C. The longest lived samples were obtained when care was taken to minimize the amount of water present in the solutions. Frozen solution samples suitable for Mössbauer spectroscopy and XAS were generated in butyronitrile solution at -60 °C, by addition of 2.5 – 5 equiv of a 0.2 M toluene solution of NOct$_4$OH. ^{1}H-NMR of **6** (CD$_3$CN, 233 K, all peaks appear as broad singlets): δ 63.1 (1H, CC*H*$_2$C), 56.0 (1H, CC*H*$_2$C), 33.2 (2H, CC*H*$_2$C + NC*H*$_2$), 30.2 (1H, CC*H*$_2$C), 20.1 (1H, NC*H*$_2$), -25.4 (1H, NC*H*$_2$), -34.9 (2H, NC*H*$_2$), -43.6 (1H, NC*H*$_2$), -48.7 (3H, N*Me*), -53.4 (3H, N*Me*), -57.3 (3H, N*Me*), -117.8 (1H, NC*H*$_2$), -132.4 (1H, NC*H*$_2$), -135.2 (1H, NC*H*$_2$), -187.1 (2H, NC*H*$_2$), -204.6 (1H, NC*H*$_2$), -252.2 (1H, NC*H*$_2$).

X-Ray Crystallography

Selected single crystals of **4** and **5** were placed onto the top of 0.1 mm diameter glass capillaries and mounted on a Bruker SMART V5.054 CCD area detector diffractometer for data collection. A preliminary set of cell constants was collected from reflections harvested from three sets of 20 frames. These initial sets of frames were oriented such that orthogonal wedges of reciprocal space were surveyed and then used to produce initial orientation matrices. Data collection was carried out using MoKα radiation (graphite monochromator) at a detector distance of 4.9 cm. A randomly oriented region of reciprocal space was surveyed to the extent of one sphere and to a resolution of 0.77 Å, with four major sections of frames being collected using 0.30° steps in ω at four different ϕ settings and a detector position of -28° in 2θ. The intensity data were corrected for absorption and decay (SADABS).[5] Final cell constants were calculated from the actual data collection after integration (SAINT).[6] Please refer to Tables S1 and S2, and Figure S2, plus accompanying text, for additional crystal and refinement information.

The structures were solved and refined using Bruker SHELXTL.[7] Space groups were determined based on systematic absences and intensity statistics. In both cases a direct-methods solution was calculated, which provided most non-hydrogen atoms from the E-map. The remaining non-hydrogen atoms were located by full-matrix least squares/difference Fourier cycles. All non-hydrogen atoms were refined with anisotropic displacement parameters. All hydrogen atoms were placed in ideal positions and refined as riding atoms with relative isotropic displacement parameters.

Crystallographic data for **4** and **5** have been deposited with the Cambridge Crystallographic Data Centre with respective deposition numbers of CCDC 964341 and 964342.

Spectroscopic Methods

NMR spectra were recorded using Varian Inova 500 MHz or 300 MHz spectrometers or a Bruker AV-500. Chemical shifts (ppm) were referenced to residual protic solvent peaks. UV-Visible studies were performed using a HP8453A diode array spectrometer equipped with a

cryostat from Unisoku Scientific Instruments (Osaka, Japan). Electrospray ionization mass spectrometry (ESI-MS) experiments were carried out on a Bruker BioTOF II mass spectrometer using a spray chamber voltage of 4000 V and a gas carrier temperature of 60 ºC. Samples of **6** for ESI-MS were prepared at -40 °C by treatment of **5** with 5 equivalents of NBu_4OH, and all transformations were monitored by UV-Vis spectroscopy. The Mössbauer spectra were recorded with a home built spectrometer, using a Janis Research (Wilmington, MA) Super Varitemp dewar. Isomer shifts are quoted relative to Fe metal at 298 K.

Resonance Raman spectra were obtained using a liquid nitrogen cooled CCD detector (model LN/CCD-1340 × 400PB, Princeton Instruments) attached to a 1-m polychrometer (model MC-100DG, Ritsu Oyo Kogaku). An excitation wavelength of 407 nm was provided by a Kr^+ laser (Spectra Physics BeamLok 2060-RM) with *ca.* 20 mW power at the samples and this laser also provided the 568 nm beam at ~ 90 mW. All measurements of **5** were carried out in frozen solution with samples mounted on a brass cold finger, and its ^{18}O-labelled isotopomer was prepared via the procedure outlined in the experimental section of the paper but using $PhI^{18}O$ as the oxidant.[8] Attempts to record spectra of **6** via similar means were unsuccessful. Instead, noisy but reproducible spectra of **6** were obtained in cooled (-20 °C) liquid solution in flat-bottomed NMR tubes, with samples being prepared via the addition of anhydrous $[NBu_4](OMe)$ to CH_3CN solutions of **5** cooled to -44 °C. (Note: recording resonance Raman spectra of **5** in liquid CH_3CN solution yielded an ν(Fe=O) at the same energy as in frozen butyronitrile solution.) Raman shifts were calibrated with indene, and the accuracy of the peak positions of the Raman bands was ± 1 cm^{-1}.

X-ray Absorption Spectroscopy.

X-ray absorption data was collected on beamlines 9-3 (**5**, 7 scans, 16 mM, quantitative yield by UV/Vis) and 7-3 (**6**, 15 scans, 6.94 mM, yield of 90% by UV/Vis) of the Stanford Synchrotron Radiation Lightsource (SSRL) of SLAC National Accelerator Laboratory with storage ring conditions of 3.0 GeV and 80 – 100 mA. Fe K-edge XAS data were collected for frozen solutions maintained at a temperature of *ca.* 15 K over an energy range of 6.9 – 8.0 keV using a Si(220) double crystal monochromator for energy selection and an Oxford Instruments CF1208 continuous flow liquid helium cryostat for temperature control. Harmonic rejection was achieved at both beamlines using a vertically collimating Rh-coated mirror located upstream of the monochromator. Data were obtained as fluorescence excitation spectra with a 30-element solid-state germanium detector array (Canberra). An iron foil spectrum was recorded concomitantly for internal energy calibration and the first inflection point of the K-edge was assigned to 7112.0 eV. The edge energies of the XAS samples were routinely monitored during data collection for red-shifts indicative of photoreduction. While **5** exhibited no evidence for photoreduction, a red-shift of ~0.5 eV was observed for **6** when a single spot was exposed to the x-ray beam for two or more hours (equivalent to 6 complete EXAFS scans). Consequently, the position of the x-ray beam was moved to a fresh portion of **6** following three complete scans at individual spots, and the averaged data reflects the sum of the first three scans only at all exposed spots.

Data reduction, averaging, and normalization were performed using the program EXAFSPAK.[9] Following calibration and averaging of the data, background absorption was

removed by fitting a Gaussian function to the pre-edge region and then subtracting this function from the entire spectrum. A three-segment spline with fourth order components was then fit to the EXAFS region of the spectrum to obtain $\chi(k)$. Analysis of the pre-edge features was carried out with the program SSExafs.[10] Theoretical phase and amplitude parameters for a given absorber-scatterer pair were calculated using FEFF 8.40[11] at the single-scattering level of theory, and were utilized by the opt program of the EXAFSPAK package during curve-fitting. In all analyses, the coordination number of a given shell was a fixed parameter, and was varied iteratively while bond lengths (r) and Debye-Waller factors (σ^2) were allowed to freely float. The amplitude reduction factor S_0 was fixed at 0.9. For each sample, E_0 (the point at which $k = 0$ $Å^{-1}$) was taken to be the first inflection point of the rising Fe K-edge, and the edge shift parameter ΔE_0 was allowed to float as a single value for all shells. ΔE_0 values were between -10 and +10 eV in all reported fits. In any given fit, the number of floating parameters = (2 × num shells) + 1. The goodness of fit F was defined simply as $\Sigma (\chi_{exptl}-\chi_{calc})^2$. In order to account for the effect that additional shells have on improving fit quality, an additional goodness-of-fit metric *F'* was employed. $F' = F^2 / (N_{IDP} - N_{VAR})$, where N_{VAR} is the number of floated variables in the fit, while N_{IDP} is the number of independent data points and is defined as $N_{IDP} = 2\Delta k \Delta r/\pi$.[12]

Computational Details

DFT calculations were performed with the Gaussian '09 software package[13] on a cluster of 8 processors using the hybrid functional B3LYP and the triple-ζ basis set 6-311G. We used tight convergence criteria (SCF=TIGHT) for the SCF procedure and default settings for the geometry optimizations. From these calculations we obtained the geometry-optimized structures of **5** and **6**, shown in Figures S13 and S14, respectively; Cartesian coordinates for **5** and **6** obtained from these calculations can be found in Tables S7 and S8, respectively. The initial coordinates of **5** used for computational studies were obtained from the X-ray crystallographic structure. Once the optimized structures were obtained, property calculations were performed using the Guassian '09 software package by including the keyword "prop". Calculated quadrupole splittings (ΔE_Q), isomer shifts (δ), and asymmetry parameters (η) (found in Table 2, main text) were determined using the calculated properties of the optimized structures for **5** and **6**. We used the conversion factor -1.7 mm s^{-1} $a.u.^{-1}$ for the calculation of quadrupole splitting parameters.

The ORCA 2.4.45 software package developed by Prof. Frank Neese[14] was used to perform single point DFT and time-dependent DFT (TD-DFT) calculations on models of **5** and **6**. The one-parameter Perdew-Burke-Erzerhoff (PBE0) hybrid functional[15] was used in conjunction with the DGauss (Gaussian polarized double-ζ valence orbital) basis as well as the Demon/J auxiliary basis[16] for all atoms except Fe and $O/N_{equatorial}$, for which Ahlrichs' polarized triple-ζ valence polarization (TZVP)[17] and double- ζ valence polarization (DZP) basis sets were used, respectively. Fifty excited states were considered in all TD-DFT calculations.

The results from TD-DFT calculations were used to simulate Abs spectra by assuming that each electronic transition gives rise to a Gaussian band with a full width at half maximum $\nu_{1/2}$ = 1,700 cm^{-1}. Isosurface plots of key molecular orbitals (MOs) and electron density

difference maps (EDDMs) were generated with the gOpenMol program developed by Laaksonen[18] using isodensity values of 0.03 au and 0.003 au, respectively.

Cyclic Voltammetry

All cyclic voltammetry experiments were performed using a BAS 100B/W Electrochemical Analyzer potentiostat, either inside a nitrogen atmosphere glove box, or under a positive pressure of argon in a vial sealed with a septum. Acetonitrile solution containing 0.1 M tetrabutylammonium hexafluorophosphate as the electrolyte, a glassy carbon working electrode, a platinum wire counter electrode, and a Ag^+/Ag reference electrode were used throughout. The latter was prepared by inserting a Ag wire into an acetonitrile solution of 0.1 M tetrabutylammonium hexafluorophosphate and 0.01 M $AgPF_6$ contained within a glass tubing capped with a porous vycor tip and heat shrink tubing (BASi, Inc., West Lafayette, IN, USA, part no. MF-2064). Temperature of measurement was maintained using a methanol/liquid nitrogen bath. All potentials are referenced against the ferrecenium/ferrocene (Fc^+/Fc) couple.

Reaction Kinetics

All kinetic studies were performed under a nitrogen atmosphere. Acetonitrile solutions of **3** and **5** (1.0 and 0.5 mM, respectively) were prepared from their iron(II) precursors using the procedure outlined above for **5**. The yields of oxoiron(IV) complex were assessed using electronic spectroscopy and found to be near quantitative in both cases. Generation of **6** was achieved by addition of 1.2-1.3 equivs of NBu_4OH dissolved in CH_3CN (0.1 mM solution prepared from $NBu_4OH{\cdot}30H_2O$, using dry solvent), relative to iron concentration. (The quantity of NBu_4OH added equates to the minimum amount required for full conversion of **5** to **6**, which was established by titration at -40 ˚C using electronic spectroscopy.) Dichloromethane solutions of the substrates PPh_3, $PMePh_2$ and 1,4-cyclohexadiene (CHD) were added in > 10-fold excess to solution of the aforementioned oxoiron(IV) complexes at 0 ˚C. The resulting reactions were monitored by decay of their respective near-IR features and found to display pseudo-first order kinetics. Plots of effective rate constants (k_{eff}) *vs*. substrate concentration were found to be linear in all cases, thereby yielding second order rate constants (k_2) (Figures S2 - S8).

Product Analysis

Products from the oxidation reactions were identified and quantified by ^1H or ^{31}P NMR (Bruker AV-500 spectrometer) of CD_3CN solutions of **3**, **5**, and **6** (0.5 or 2 mM) to which substrate was added at 0 °C. The ^{31}P NMR delay time was lengthened to 30 seconds for sufficient relaxation of the resonances to allow proper integration of the phosphorus peaks. The NMR spectra of samples with just CD_3CN and organic reactant were obtained for comparison. The amounts of product generated were compared with the concentration of the iron(IV)-oxo complex determined by measuring its absorbance at the appropriate λ_{max} by UV-vis spectroscopy.

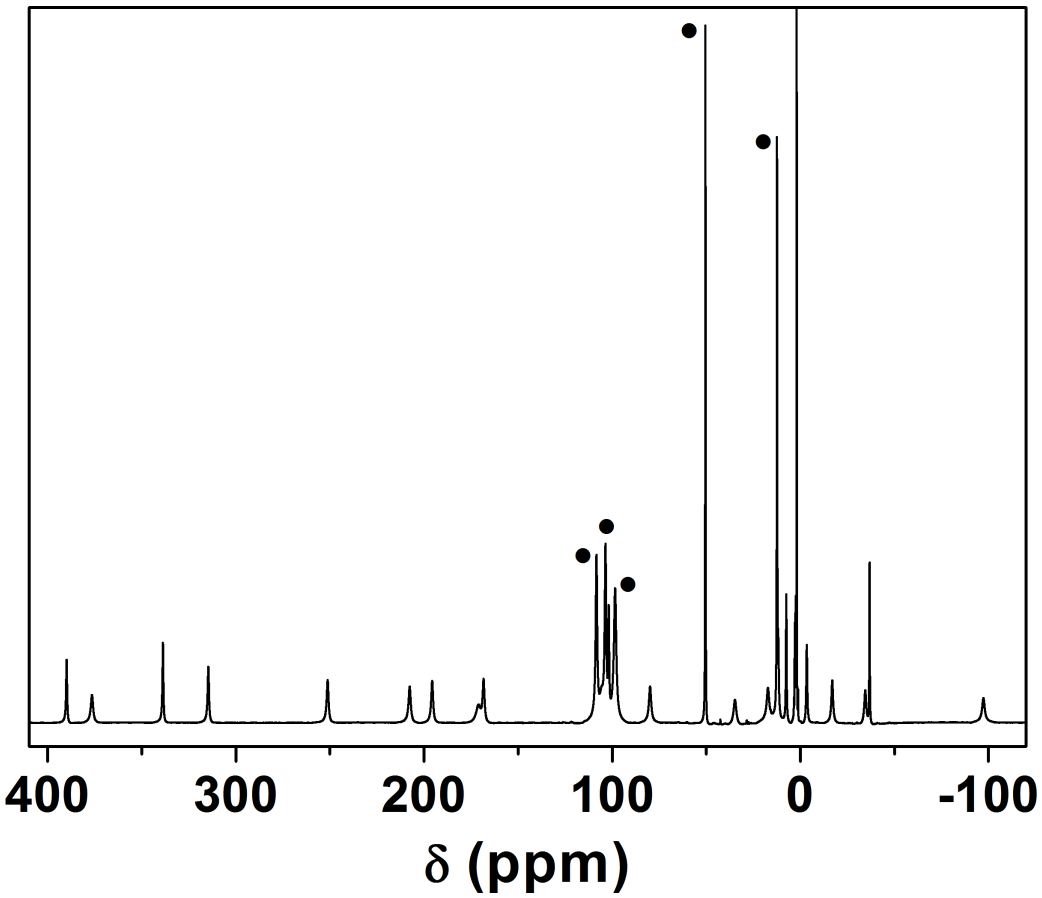

Figure S1. ^{1}H NMR spectrum of [Fe^{II}(1,4,8-Me_3cyclam-11-$CH_2C(O)NMe_2$)](OTf)$_2$ (**4**) recorded in CD_3CN solution at ambient temperature. Acquisition time = 0.064 sec.; relaxation delay = 0.03 sec.; line broadening factor = 30 Hz. Resonances corresponding to the methyl substituents are labeled with •, and further peak assignments are provided in the synthetic section on page S2. A few words describing the rationale used for peak assignments are provided below.

Complex **4** is C_1 symmetric, so we expect all 22 methylene protons and the 5 methyl substituents (3 protons each) to be magnetically inequivalent. This should yield 27 resonances, with the methyl groups easily identifiable by peak integration. The spectrum of **4** contains a total of only 25 distinct resonances, but full peak integration indicates that resonances corresponding to all 37 protons in the ligand are present. In this instance, two of the methyl peaks integrate to 4 protons each and display asymmetry, which stems in both cases from overlap with a single methylene (1 × H) resonance.

In ^{1}H NMR spectra of paramagnetic complexes, the half-height line width ($\nu_{1/2}$) of a peak is inversely related to the transverse spin-spin relaxation time (T_2). Assuming a through-space dipolar interaction between the nuclear and electronic magnetic moments is the predominant mechanism for nuclear relaxation, which is usually the case, T_2 is itself proportional to r^6 (r = the distance of the proton away from the metal center). Consequently, peaks of protons close to the metal center experience severe line broadening, but protons far away yield sharp peaks. With this in mind, the two methyl groups of the NMe_2 group are readily identified as corresponding to the resonances at 50.5 and 12.4 ppm. Assignment of the non-methyl peaks to specific methylene protons is much more difficult; as such an effort would be of limited value here, so it was not pursued.

Using the rationale and generalizations outlined above, peak assignments can also be made for the NMR of spectra of **5** and **6**. The room temperature (RT) NMR spectrum of **5**, plus assignment of its peaks, is provided below (Figure S2). Unlike in the case of **4**, integration of all peaks in the room temperature spectrum of **5** located only 35 protons (i.e., two were missing). The five methyl substituents are easily identified by peak integration, with those of the $C(O)NMe_2$ pendant arm being discerned from the others due to their very narrow line widths, and all are strongly paramagnetically shifted. Therefore, "misplacing" two protons due to a rapid chemical equilibrium resulting from coordination/loss of the pendant arm, which would presumably also causing broadening of the $C(O)NMe_2$ resonances, seems very unlikely. Instead, severe line broadening due to very repaid nuclear relaxation, which complicates accurate peak integration and can even lead to the resonances being imperceptible, is a more likely cause.

Once again, assignment of the methylene protons is less than straightforward and of debatable merit, so minimal effort was made in this regard. However, the four peaks at 46.6, 40.2, 27.3 and 25.2 ppm corresponding to 1 H each are noticeably sharper than those of the other methylene protons, which suggests that they are on the relatively remote 6- and 13-C atoms of the tetraazacyclam ring (i.e., NC*CH*$_2$CN). Support for this notion was provided using COSY, which showed coherence between the pair of peaks at 46.6 and 27.3 ppm, and those at 40.2 and 25.2 ppm (Figure S3).

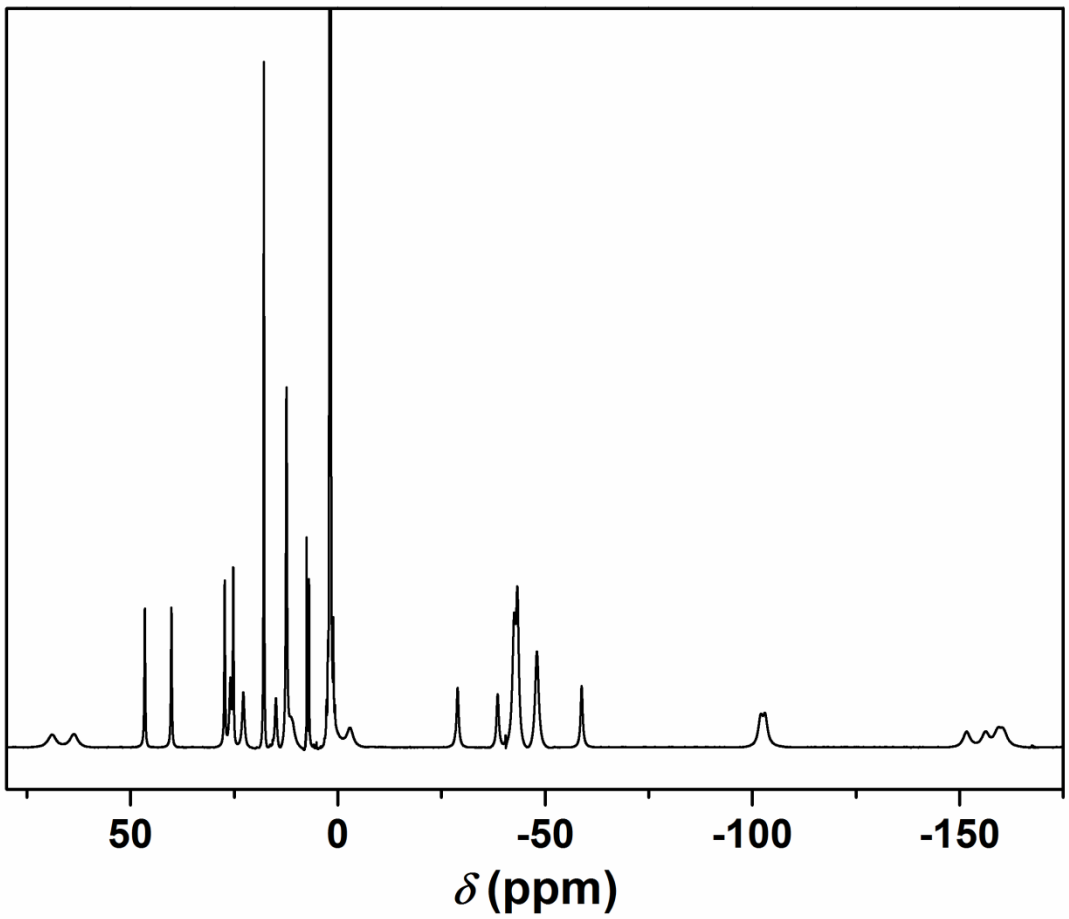

Figure S2. ^{1}H NMR spectra of **5** recorded in CD_3CN solution at room temperature. Acquisition time = 0.064 sec.; relaxation delay = 0.03 sec.; line broadening factor = 30 Hz. Peak assignments are as follows: δ 68.9 (1H, NC*H*$_2$), 63.7 (1H, NC*H*$_2$), 46.6 (1H, CC*H*$_2$C), 40.2 (1H, CC*H*$_2$C), 27.3 (1H, CC*H*$_2$C), 25.9 (1H, NC*H*$_2$), 25.2 (1H, CC*H*$_2$C), 22.8 (1H, NC*H*$_2$), 17.8 (3H, C(O)N*Me*), 14.9 (1H, NC*H*$_2$), 12.4 (3H, C(O)N*Me*), 11.3 (1H, NC*H*$_2$), -3.0 (1H, NC*H*$_2$), -28.9 (1H, NC*H*$_2$), -38.5 (1H, NC*H*$_2$), -42.5 (3H, N*Me*), -43.3 (3H, N*Me*), -48.0 (3H, N*Me*), -58.8 (1H, NC*H*$_2$), -102.1 (1H, NC*H*$_2$), -103.0 (1H, NC*H*$_2$), -151.7 (1H, NC*H*$_2$), -156.3 (1H, NC*H*$_2$), -159.5 (2H, NC*H*$_2$).

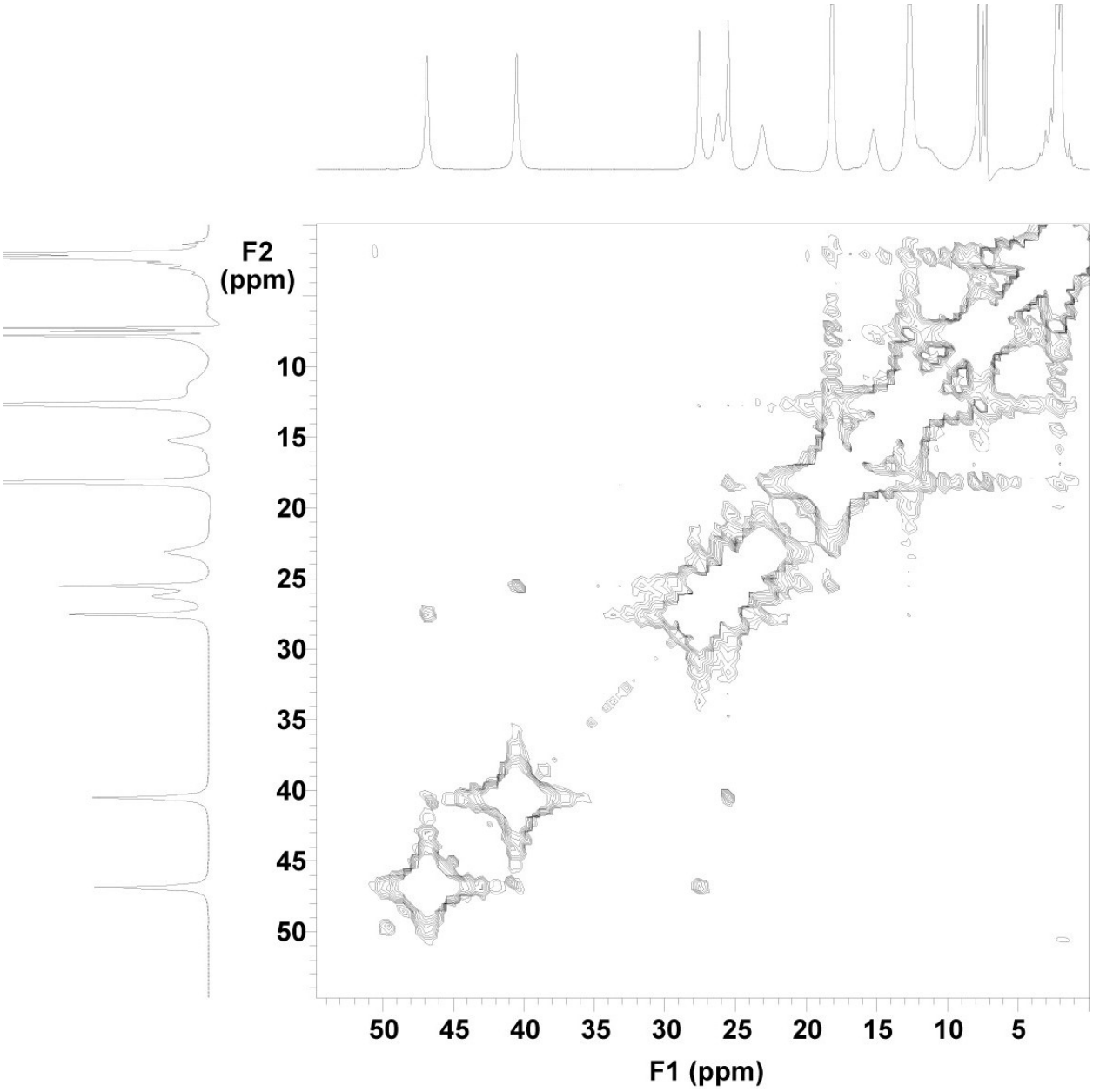

Figure S3. ^{1}H NMR COSY of **5** recorded in CD_3CN solution at room temperature. Acquisition time = 0.064 sec.; relaxation delay = 0.03 sec.; line broadening factor = 30 Hz.

To allow comparison with the ^{1}H NMR spectrum of **6**, which is only stable at low temperatures, that of **5** was also recorded at -40˚C and appears in Figure 3 in the main text. As expected based upon Curie's Law, all peaks appear at greater δ values (see synthesis section on

page S2) and are broader than in the RT spectrum. However, using peak integration and comparison with the RT spectrum, it is apparent that all resonances are still present, which means that two ligand protons still cannot be accounted for. The spectrum of **6** was recorded at -40˚C (Figure 3 in the main text) and peaks assigned using the means described above. In this case, integration of all peaks left four methylene protons and two methyl groups unaccounted for (due to deprotonation of the NCH_2C(O) linker we expect a total of 36 protons). The absence of the former can once again be rationalized by severe line broadening effects due to very rapid nuclear relaxation. On the other hand, the two missing methyl resonances are likely to be in the diamagnetic region and obscured by solvent, water, NBu_4^+ and PhI signals. While this could be due to decoordination of the amide pendant arm, **6** exhibits a number of properties that would be difficult to explain if one assumes metathesis to yield a hydroxide complex. Instead it seems more likely that these peaks simply shifted into the diamagnetic region due to decreased delocalization of spin density onto the NMe_2 unit, or by a change in the mechanism of spin delocalization.

Crystallographic data for complexes 3 and 4

The structure of **4** (Figure S2) was found to contain two formula units per asymmetric unit: Z' = 2. While the space group symmetry is $P2_1/c$ in the monoclinic crystal system, there is strong pseudo-symmetry between the dications and at least one pair of the triflate anions resulting in a pseudo-2_1 parallel to *a* axis. Given the crystallographic symmetry operations in $P2_1/c$, a pseudo-glide and a pseudo-inversion center are also expected. The unit cell is very close to being metrically orthorhombic. The structure was found to be a pseudo-merohedral twin. It was arbitrarily modeled with a 180º rotation about the *a* axis. This reduced the R1 from over 0.10 to the present value.

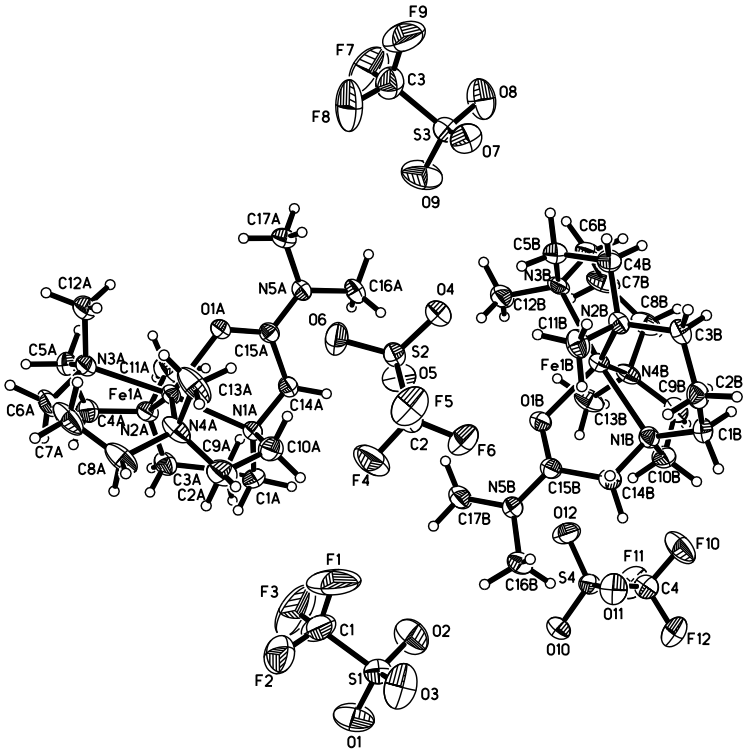

Figure S4. Thermal ellipsoid drawing of $[Fe^{II}(1,4,8\text{-}Me_3cyclam\text{-}11\text{-}CH_2C(O)NMe_2)](OTf)_2$ (**4**), showing 50 % probability ellipsoids.

Table S1. Crystal data and structure refinement for [Fe^{II}(1,4,8-Me_3cyclam-11-$CH_2C(O)NMe_2$)](OTf)$_2$ (**4**), deposited with the CCDC as CDCC 964341.

Identification code	07286b	
Empirical formula	C_{19} H_{37} F_6 Fe N_5 O_7 S_2	
Formula weight	681.51	
Temperature	173(2) K	
Wavelength	0.71073 Å	
Crystal system	Monoclinic	
Space group	$P2_1/c$	
Unit cell dimensions	a = 14.6683(14) Å	α = 90°
	b = 28.684(3) Å	β = 90.199(2)°
	c = 13.8712(13) Å	γ = 90°
Volume	5836.2(10) Å^3	
Z	8	
Density (calculated)	1.551 Mg/m^3	
Absorption coefficient	0.744 mm^{-1}	
F(000)	2832	
Crystal color, morphology	Colorless, Plate	
Crystal size	0.45 x 0.40 x 0.08 mm^3	
Theta range for data collection	0.71 to 27.52°	
Index ranges	$-18 \le h \le 18$, $0 \le k \le 36$, $0 \le l \le 17$	
Reflections collected	67258	
Independent reflections	13275 [R(int) = 0.0500]	
Observed reflections	9141	
Completeness to theta = 27.52°	98.9%	
Absorption correction	Multi-scan	
Max. and min. transmission	0.9429 and 0.7306	
Refinement method	Full-matrix least-squares on F^2	
Data / restraints / parameters	13275 / 0 / 732	
Goodness-of-fit on F^2	1.019	
Final R indices [I>2sigma(I)]	$R1$ = 0.0478, $wR2$ = 0.0984	
R indices (all data)	$R1$ = 0.0788, $wR2$ = 0.1078	
Largest diff. peak and hole	0.667 and -0.377 e.Å^{-3}	

Table S2. Crystal data and structure refinement for $[Fe^{IV}(O)(1,4,8\text{-}Me_3cyclam\text{-}11\text{-}CH_2C(O)NMe_2)](OTf)_2$ (**5**), deposited with the CCDC as CDCC 964342.

Identification code	07217a	
Empirical formula	$C_{19}\ H_{37}\ F_6\ Fe\ N_5\ O_8\ S_2$	
Formula weight	697.51	
Temperature	123(2) K	
Wavelength	0.71073 Å	
Crystal system	Monoclinic	
Space group	$P2_1/n$	
Unit cell dimensions	a = 12.4264(12) Å	α = 90°
	b = 11.0862(10) Å	β = 94.500(2)°
	c = 20.4399(19) Å	γ = 90°
Volume	2807.2(5) Å^3	
Z	4	
Density (calculated)	1.650 Mg/m^3	
Absorption coefficient	0.778 mm^{-1}	
F(000)	1448	
Crystal color, morphology	Brown, Plate	
Crystal size	0.45 x 0.20 x 0.06 mm^3	
Theta range for data collection	1.86 to 27.50°	
Index ranges	$-16 \le h \le 16$, $0 \le k \le 14$, $0 \le l \le 26$	
Reflections collected	6431	
Independent reflections	6431 [R(int) = 0.0000]	
Observed reflections	5224	
Completeness to theta = 27.50°	99.6%	
Absorption correction	Multi-scan	
Max. and min. transmission	0.9548 and 0.7208	
Refinement method	Full-matrix least-squares on F^2	
Data / restraints / parameters	6431 / 0 / 375	
Goodness-of-fit on F^2	1.075	
Final R indices [I>2sigma(I)]	$R1$ = 0.0343, $wR2$ = 0.0836	
R indices (all data)	$R1$ = 0.0455, $wR2$ = 0.0878	
Largest diff. peak and hole	0.476 and -0.327 e.Å^{-3}	

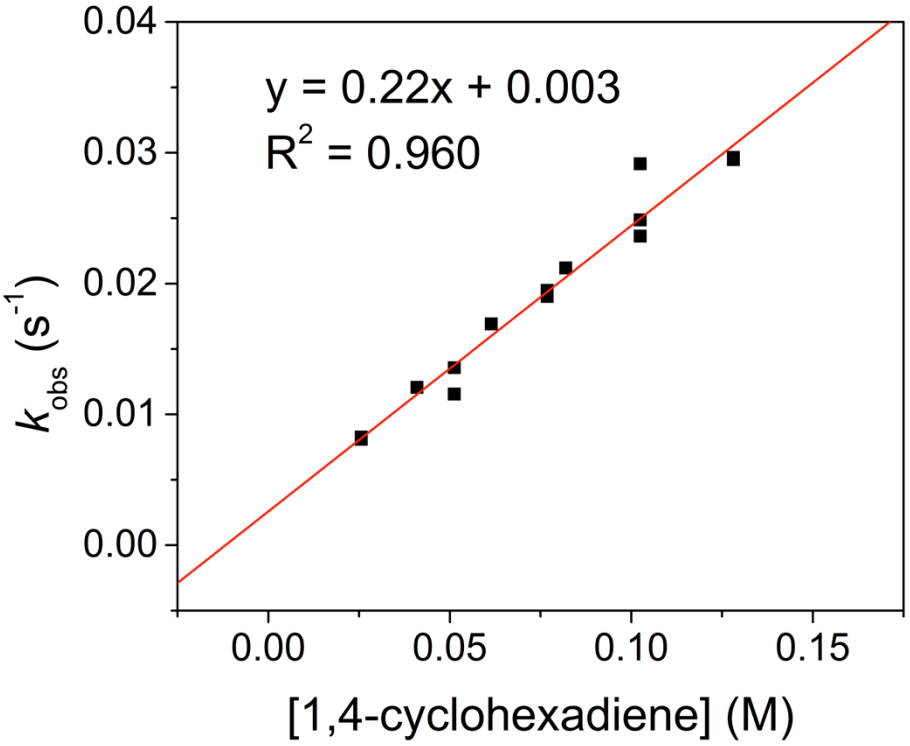

Figure S5. Plot of k_{obs} (s^{-1}) versus substrate concentration for reaction of **3** with 1,4-CHD at 0˚C.

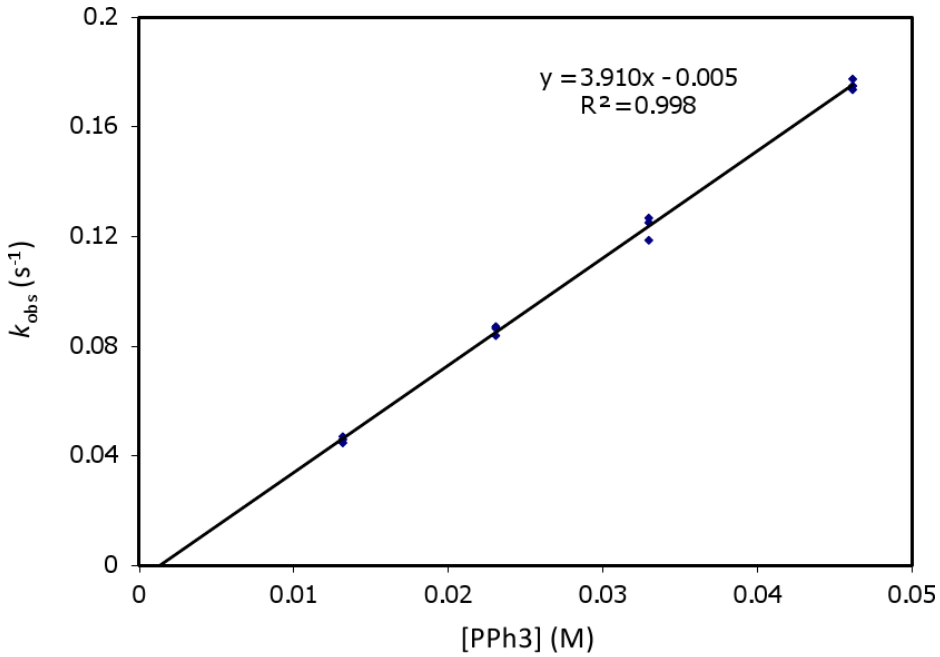

Figure S6. Plot of k_{obs} (s^{-1}) versus substrate concentration for reaction of **3** with PPh_3 at 0˚C.

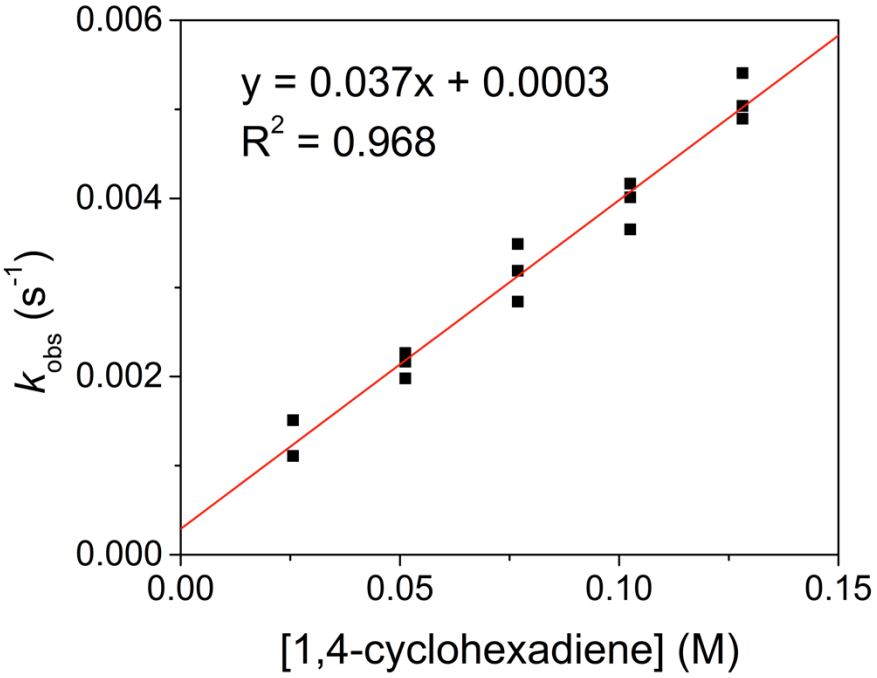

Figure S7. Plot of k_{obs} (s^{-1}) versus substrate concentration for reaction of **5** with 1,4-CHD at 0˚C.

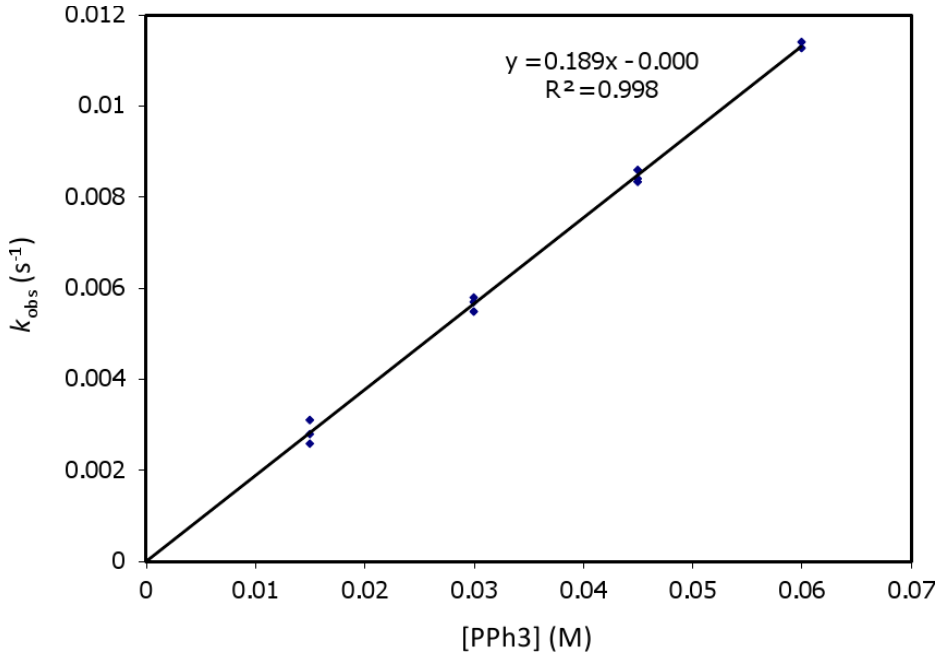

Figure S8. Plot of k_{obs} (s^{-1}) versus substrate concentration for reaction of **5** with PPh_3 at 0˚C.

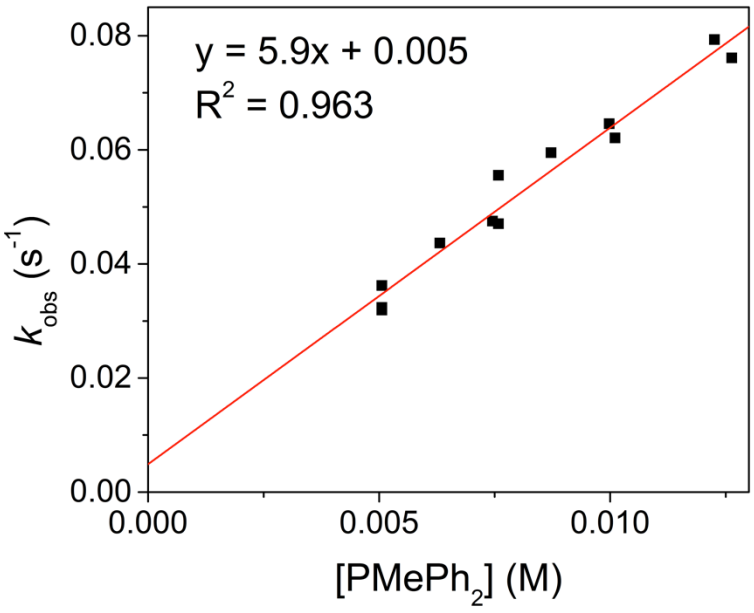

Figure S9. Plot of k_{obs} (s^{-1}) versus substrate concentration for reaction of **5** with $PMePh_2$ at 0˚C.

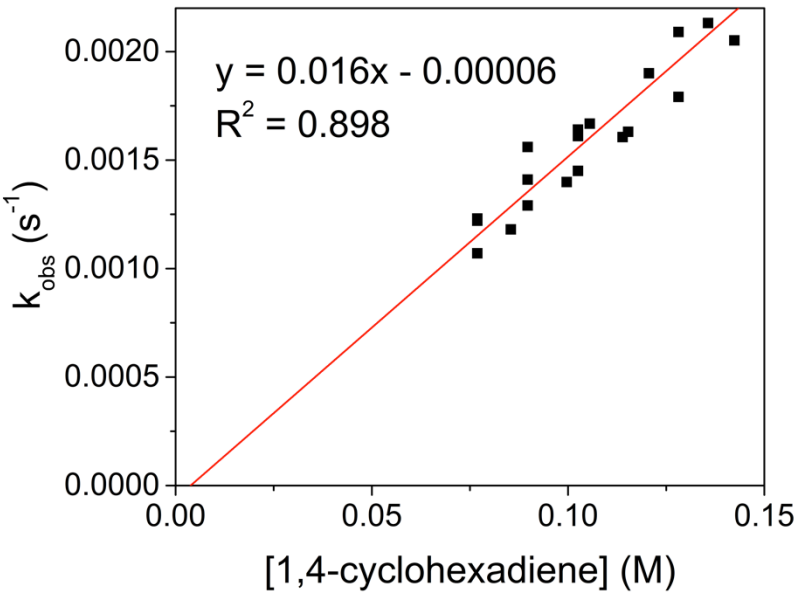

Figure S10. Plot of k_{obs} (s^{-1}) versus substrate concentration for reaction of **6** with 1,4-CHD at 0˚C.

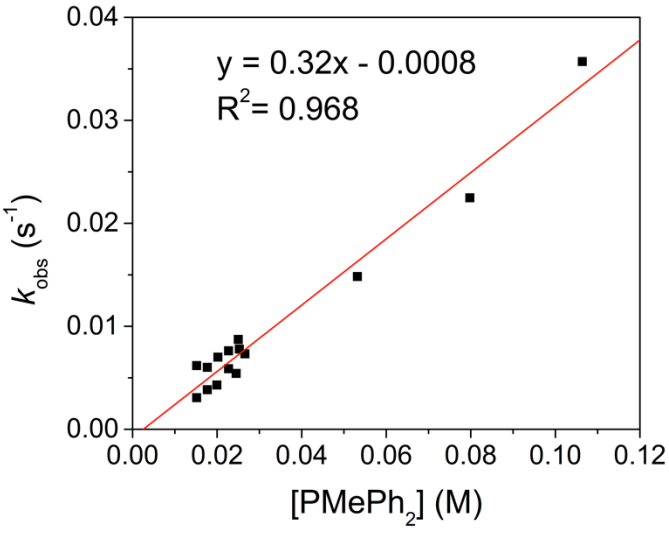

Figure S11. Plot of k_{obs} (s^{-1}) versus substrate concentration for reaction of **6** with $PMePh_2$ at 0˚C.

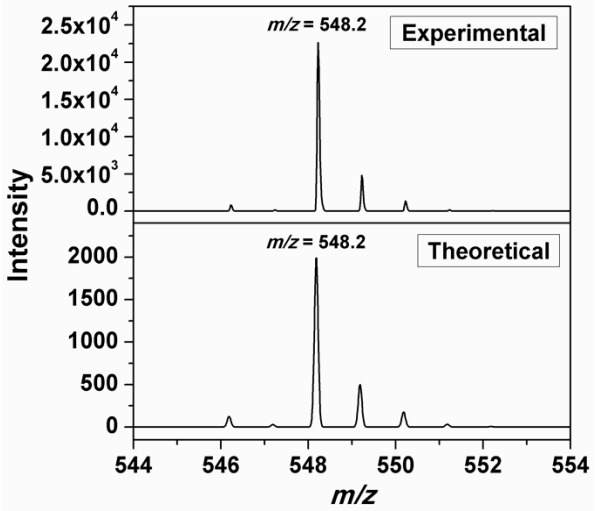

Figure S12. The electrospray ionization mass spectrum (ESI-MS) of $[Fe^{IV}(O)(Me_3cyclam\text{-}CH_2C(O)NMe_2)](OTf)_2$ (**5**), showing the observed (top) and expected (bottom) isotope distribution patterns for the ion fragment $\{[Fe^{IV}(O)(1,4,8\text{-}Me_3cyclam\text{-}11\text{-}CH_2C(O)NMe_2)](OTf)\}^+$.

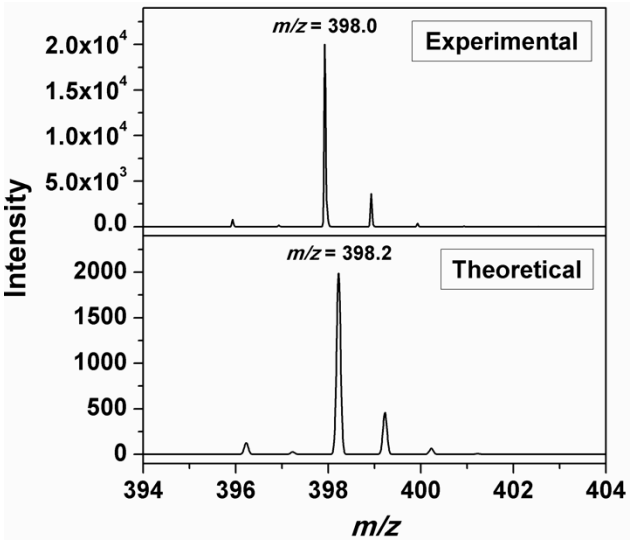

Figure S13. The electrospray ionization mass spectrum (ESI-MS) of **6**, prepared at -40°C by treatment of $[Fe^{IV}(O)(1,4,8\text{-}Me_3cyclam\text{-}11\text{-}CH_2C(O)NMe_2)](OTf)_2$ (**5**) with 5 equivalents of NBu_4OH, showing the observed (top) and expected (bottom) isotope distribution patterns for the ion fragment $\{[Fe^{IV}(O)(1,4,8\text{-}Me_3cyclam\text{-}11\text{-}CH_2C(O)NMe_2)] - H\}^+$.

X-ray Absorption Spectroscopy of 5 and 6

XANES Analysis Parameters

Table S3. Pre-edge Analysis Parameters for **5** and **6**.[a]

Species	yield	E_{edge} (eV)	$E_{preedge}$ (eV)	height	width	area
5	100%	7125.91	7114.18(1)	0.116(1)	2.45(2)	30.4(3)
6	90%	7125.83	7114.14(1)	0.079(1)	2.44(2)	20.6(2) [23][b]

[a] The fits presented are those that give the best agreement to the experimental data and its second derivative. Values in parentheses represent uncertainties in the final digit of that parameter.
[b] The value given in square brackets is the weighted pre-edge areas that would be expected for a quantitative sample of **5**, assuming that any other species present do not contribute significantly to observed pre-edge intensity.

EXAFS Analysis of 5 and 6

The results of our EXAFS analysis of **5** are summarized in Tables S4 and S6 and Figure S12. Analysis of Fourier-filtered EXAFS data reveals that the first-shell features of **5** are best modeled with 5 Fe–N/O scatterers at 2.03 Å associated with the equatorial nitrogens of the TMC ligand and the axial amide oxygen donor, along with 1 Fe–O/N scatterer at 1.63 Å, readily assignable to the Fe=O moiety (fit 7, Table S4). These values are in good agreement with the values obtained from X-ray crystallographic analysis of 2.044 Å and 1.6579(13) Å for the average Fe–N_{eq}/O_{amide} and Fe=O bond lengths, respectively. A fit in which the principal Fe–N/O shell was split into two subshells consisting of 4 Fe–N at 2.06 Å and 1 Fe–O at 1.96 Å afforded a decrease in fit quality and unreasonable σ^2 values (fit 8, Table S4). Moreover, the difference in bond lengths of 0.10 Å is smaller than the resolution limitation of 0.12 Å for atoms of similar *Z* imposed by the *k*-range of the EXAFS data for **5**. Analysis of the outer-shell features indicates that they can be most simply modeled by 5 Fe•••C scatterers at approximately 2.98 Å (fit 15, Table S4), but a more elaborate fit consisting of three distinct shells of Fe•••C scatterers at 2.88, 3.02, and 3.49 Å affords moderate improvements in fit quality and visual agreement between the experimental and calculated $k^3\chi(k)$ spectra (fit 25, Table S4, Figure S12). An identical

progression of best fits is obtained for an analysis of unfiltered $k^3\chi(k)$ EXAFS data, as summarized in Table S5 and Figure S12.

The first coordination sphere of **6** is best fit to 5 Fe–N/O scatterers at *ca.* 2.03 - 2.04 Å and 0.9 Fe–O/N scatterer at 1.67 Å (fit 33a, Table S6), with the lengthening of the Fe=O bond length relative to **5** being in accord with the greater basicity of the ligand *trans* to the oxo. Both distances are in reasonably good agreement with the average $Fe–N_{eq}/O_{amide}$ bond length of 2.07 Å and Fe=O bond length of 1.667 Å obtained for a geometry optimized DFT structure. DFT studies predicted a considerable shortening of the axial $Fe–O_{amide}$ bond length in **6** compared to **5**, and thus we expected to be able to resolve this subshell in our EXAFS analysis of **6**. However, all attempts to do so were unsuccessful, as splitting of the principal Fe–N/O shell universally afforded poorer goodness-of-fit parameters and unreasonable σ^2 values for the presumptive $Fe–O_{amide}$ shell (fits 34-40, Table S6). We do note that the magnitude of σ^2 for the Fe–N/O shell is significantly larger for **6** (5.4×10^{-3} Å^2) compared to **5** (2.8×10^{-3} Å^2), which would imply greater static disorder in this shell for **6** due to a larger spread of bond lengths. The weak outer-shell features observed in the Fourier transform of the EXAFS data of **6** are best modeled by three distinct Fe•••C shells at 2.84, 3.01, and 3.42 Å (fit 56, Table S6 and Figure S13). In particular, we note that inclusion of the long 3.4 Fe•••C shell affords significant improvements in fit quality and is required to accurately model the shoulder in the $k^3\chi(k)$ EXAFS data at k = 5 Å^{-1} (compare fits 42, 46 with fits 51, 56 in Figure S13).

Table S4. Analysis of Fourier-filtered EXAFS Data of **5**.[a]

	Fe-N/O			Fe-O/N			Fe•••C				
fit	n	r	σ^2	n	r	σ^2	n	r	σ^2	F [b]	*F'* [b]
1	2	2.03	-0.2							327.9	1.250
2	3	2.04	1.0							230.8	0.619
3	4	2.04	2.1							197.2	0.452
4	5	2.03	3.1							206.7	0.497
5	6	2.04	4.1							255.9	0.761
6	4	2.04	1.9	1	1.63	2.3				63.0	0.060
7	*5*	*2.04*	*3.0*	*1*	*1.63*	*2.5*				*55.3*	*0.046*
8	4 1	2.06 1.96	1.0 -1.3	1	1.63	2.7				50.4	0.055
9	4	2.04	2.0							286.1	0.484
10	5	2.04	3.0							299.3	0.530
11	4	2.04	1.8	1	1.63	2.1				144.2	0.140
12	5	2.04	2.9	1	1.63	2.3				139.9	0.131
13	5	2.04	2.9	1	1.63	2.3	3	2.98	4.8	89.6	0.062
14	5	2.04	2.9	1	1.63	2.3	4	2.98	6.4	85.4	0.057
15	*5*	*2.04*	*2.9*	*1*	*1.63*	*2.3*	*5*	*2.98*	*7.9*	*84.4*	*0.055*
16	5	2.04	2.9	1	1.63	2.2	6	2.97	9.2	85.9	0.057
17	5	2.04	2.9	1	1.63	2.2	7	2.97	10.8	89.6	0.062
18	5	2.04	2.9	1	1.63	2.2	5 1	2.97 3.44	8.0 0.9	74.9	0.051
19	5	2.04	2.9	1	1.63	2.2	5 2	2.97 3.45	8.0 3.7	71.4	0.047
20	5	2.04	2.9	1	1.63	2.2	5 3	2.98 3.47	8.0 6.6	69.5	0.044
21	5	2.04	2.9	1	1.63	2.3	5 4	2.97 3.48	8.1 9.4	68.4	0.043
22	5	2.04	2.8	1	1.63	2.1	3 2	2.91 3.04	4.3 0.6	76.8	0.054
23	5	2.04	2.8	1	1.63	2.1	3 3	2.89 3.03	4.2 1.9	78.2	0.056
24	5	2.04	2.8	1	1.63	2.1	2 3	2.88 3.02	2.0 1.6	76.6	0.054
25	***5***	***2.03***	***2.8***	***1***	***1.63***	***2.0***	***2*** ***3*** ***2***	***2.88*** ***3.02*** ***3.44***	***1.9*** ***1.6*** ***3.2***	***61.3***	***0.042***

[a] Fourier transform range k = 2.0 – 15.0 Å^{-1} (resolution = 0.12 Å). r is in units of Å; σ^2 is in units of 10^{-3} Å^2. All fits shown here were to Fourier-filtered data employing back transformation ranges of 0.7-2.1 Å (fits 1-8) and 0.7-3.1 Å (fits 9-25).

[b] Goodness-of-fit parameter F defined as $\Sigma(\chi_{exptl}-\chi_{calc})^2$. A second parameter, *F'*, is defined as $F' = F^2 / \nu$, where $\nu = N_{IDP} - N_{VAR}$. N_{IDP} is the number of independent data points, while N_{VAR} is the number of floated variables in each optimization step. The values of *F'* shown have been divided by a factor of 10^4 for convenience. *F'* is a measure of whether an added shell significantly improves the fit.

Table S5. Analysis of Unfiltered EXAFS Data of **5**.[a]

	Fe-N/O			Fe-O/N			Fe•••C				
fit	**n**	**r**	**σ^2**	**n**	**r**	**σ^2**	**n**	**r**	**σ^2**	**F [b]**	***F'* [b]**
26	4	2.04	2.0							710.6	2.988
27	5	2.04	3.0							737.1	3.215
28	4	2.04	1.8	1	1.63	1.9				425.0	1.212
29	5	2.04	2.9	1	1.63	2.1				407.8	1.116
30	5	2.04	2.9	1	1.63	2.1	4	2.98	6.5	303.6	0.715
31	*5*	*2.04*	*2.9*	*1*	*1.63*	*2.1*	*5*	*2.97*	*7.9*	*302.2*	*0.708*
32	5	2.04	2.9	1	1.63	2.1	6	2.97	9.4	306.0	0.726
33	5	2.04	2.8	1	1.63	2.0	3 2	2.91 3.04	4.1 0.9	291.4	0.779
34	5	2.04	2.8	1	1.63	2.0	2 3	2.88 3.02	2.4 2.2	291.7	0.781
35	5	2.04	2.8	1	1.63	2.0	3 3	2.89 3.03	4.6 2.5	294.8	0.797
36	***5***	***2.04***	***2.8***	***1***	***1.63***	***2.0***	***2*** ***3*** ***2***	***2.88*** ***3.02*** ***3.49***	***2.4*** ***2.2*** ***7.0***	***269.0***	***0.813***

[a] Fourier transform range k = 2.0 – 15.0 Å^{-1} (resolution = 0.12 Å). r is in units of Å; σ^2 is in units of 10^{-3} Å^2. All fits shown are for unfiltered EXAFS data.

[b] Goodness-of-fit parameter F defined as $\Sigma(\chi_{exptl}-\chi_{calc})^2$. A second parameter, F', is defined as $F' = F^2 / \nu$, where $\nu = N_{IDP} - N_{VAR}$. N_{IDP} is the number of independent data points, while N_{VAR} is the number of floated variables in each optimization step. The values of F' shown have been divided by a factor of 10^4 for convenience. F' is a measure of whether an added shell significantly improves the fit.

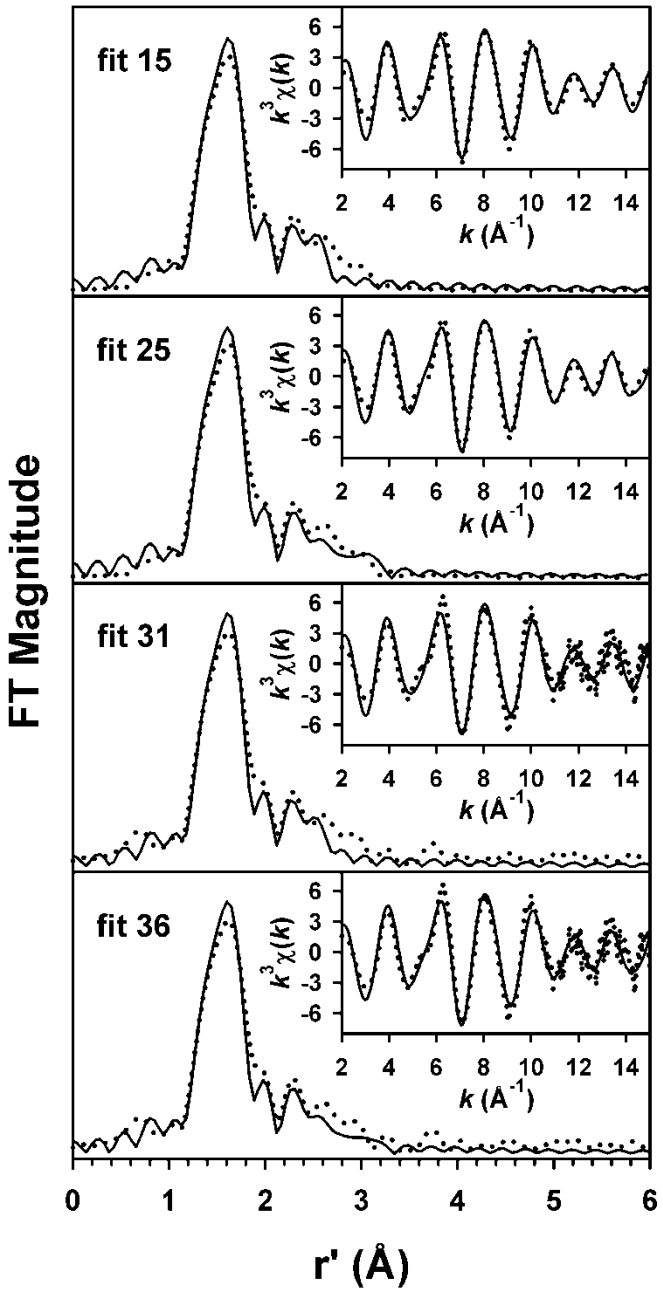

Figure S14. Fits to the Fourier transforms of the Fe K-edge EXAFS data ($k^3\chi(k)$) and either Fourier-filtered or unfiltered EXAFS spectra ($k^3\chi(k)$, insets) for **5**. Experimental data is shown with dotted lines (•••), while fits are shown with solid lines (——). Fourier transformation range: k = 2 – 15 Å^{-1}; back-transformation range: 3.1 – 0.7 Å. Fit parameters associated with the stated fit are shown in Table S4 (Fourier-filtered) or Table S5 (unfiltered).

Table S6. Analysis of Unfiltered EXAFS Data of **6**.[a]

	Fe-N/O			Fe-O/N			Fe•••C			Fe•••C				
Fit	**n**	**r**	**σ^2**	**n**	**r**	**σ^2**	**n**	**r**	**σ^2**	**n**	**r**	**σ^2**	**F** [b]	***F'*** [b]
27	3	2.04	2.5										421.5	1.110
28	4	2.04	3.9										406.5	1.033
29	5	2.04	5.3										445.9	1.243
30	6	2.04	6.8										524.4	1.719
31	3	2.04	2.3	1	1.66	2.4							302.6	0.654
31a	3	2.04	2.2	0.9	1.66	1.7							285.1	0.581
32	4	2.04	3.9	1	1.66	2.8							233.1	0.388
32a	4	2.04	3.9	0.9	1.66	2.2							224.7	0.361
33	5	2.03	5.4	1	1.67	3.0							213.6	0.326
33a	*5*	*2.04*	*5.4*	*0.9*	*1.67*	*2.4*							*213.2*	*0.325*
34	4 1	2.04 2.22	3.9 27.2	0.9	1.67	2.2							210.1	0.368
35	3 1	2.00 2.09	2.1 -0.3	0.9	1.66	2.8							221.3	0.408
36	3 2	2.03 2.02	3.1 14.0	0.9	1.66	2.1							229.4	0.439
37	4 1	2.07 1.98	5.7 0.6										440.8	1.388
38	4 1	2.04 2.22	3.9 27.9	0.9	1.66	2.2							210.1	0.368
39	3 1	2.08 1.96	0.9 -1.8										387.4	1.072
40	3 1	2.05 1.98	3.5 4.5	0.9	1.66	2.3							232.5	0.450
41	5	2.03	5.4	0.9	1.67	2.4	3	2.95	9.1				178.6	0.266
42	*5*	*2.03*	*5.4*	*0.9*	*1.67*	*2.5*	*4*	*2.94*	*11.5*				*179.9*	*0.270*

43	5	2.03	5.4	0.9	1.67	2.4	5	2.93	13.5				184.7	0.284
44	5	2.03	5.4	0.9	1.67	2.6	4 2	2.85 3.02	9.5 1.8				180.1	0.324
45	5	2.03	5.4	0.9	1.67	2.6	4 3	2.83 3.01	8.4 3.3				185.7	0.345
46	*5*	*2.03*	*5.4*	*0.9*	*1.67*	*2.5*	*3* *3*	*2.82* *3.00*	*6.0* *3.3*				*179.7*	*0.323*
47	5	2.03	5.4	0.9	1.67	2.5	3 2	2.85 3.02	7.0 1.6				172.5	0.298
48	5	2.03	5.4	0.9	1.67	2.4	4	2.94	11.7	2	3.42	1.8	140.5	0.197
49	5	2.03	5.4	0.9	1.67	2.4	4	2.95	11.7	3	3.42	3.5	133.0	0.177
50	5	2.03	5.4	0.9	1.67	2.4	4	2.95	11.5	4	3.43	5.0	128.8	0.166
51	*5*	*2.03*	*5.4*	*0.9*	*1.67*	*2.4*	*4*	*2.95*	*11.5*	*5*	*3.43*	*6.6*	*127.1*	*0.162*
52	5	2.03	5.4	0.9	1.67	2.4	4	2.96	11.4	6	3.44	8.3	127.2	0.162
53	5	2.03	5.4	0.9	1.67	2.5	4	2.96	11.2	7	3.44	10.2	128.7	0.166
54	5	2.03	5.4	0.9	1.67	2.6	4 2	2.87 3.03	10.1 2.0	5	3.42	6.0	116.7	0.170
55	5	2.03	5.4	0.9	1.67	2.5	3 2	2.86 3.02	7.2 1.5	5	3.43	5.9	115.0	0.165
56	***5***	***2.03***	***5.4***	***0.9***	***1.67***	***2.5***	***3*** ***3***	***2.84*** ***3.01***	***6.1*** ***3.2***	***5***	***3.42***	***6.1***	***116.0***	***0.168***

[a] Fourier transform range k = 2.0 - 14.0 Å^{-1} (resolution = 0.13 Å). r is in units of Å; σ^2 is in units of 10^{-3} Å^2. All fits shown are for unfiltered EXAFS data.

[b] Goodness-of-fit parameter F defined as $\Sigma(\chi_{exptl}-\chi_{calc})^2$. A second parameter, F', is defined as $F' = F^2 / \nu$, where $\nu = N_{IDP} - N_{VAR}$. N_{IDP} is the number of independent data points, while N_{VAR} is the number of floated variables in each optimization step. The values of F' shown have been divided by a factor of 10^4 for convenience. F' is a measure of whether an added shell significantly improves the fit.

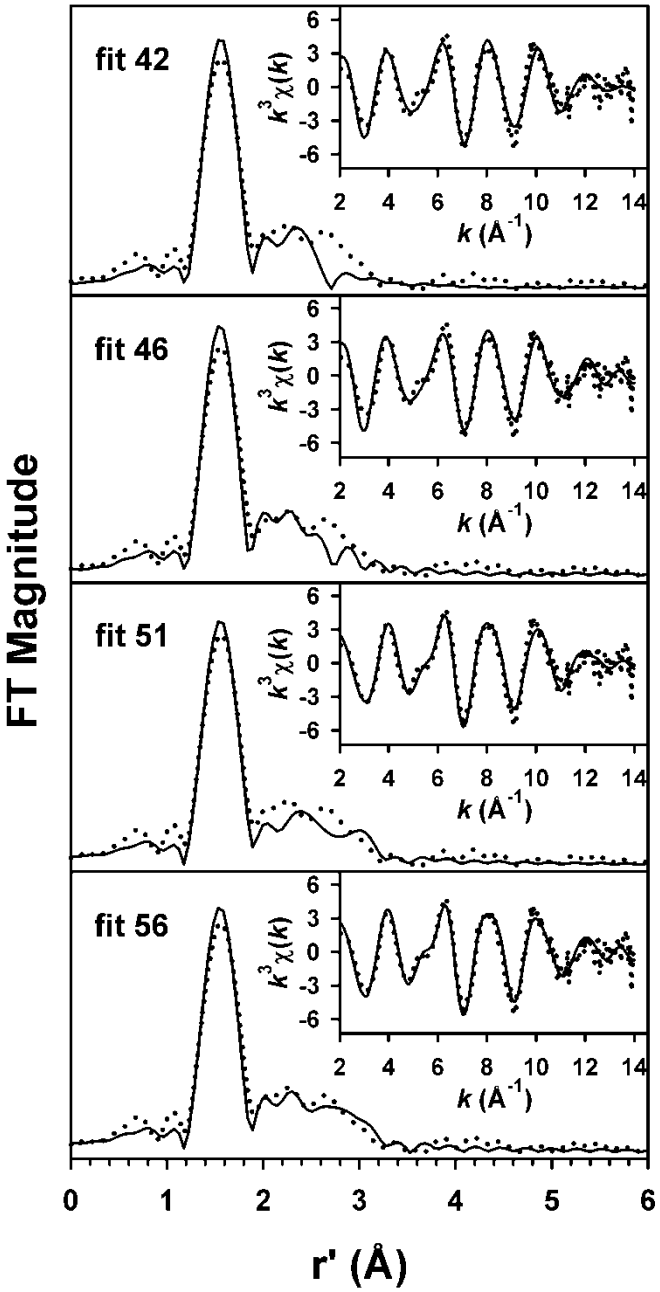

Figure S15. Fits to the Fourier transforms of the Fe K-edge EXAFS data ($k^3\chi(k)$) and unfiltered EXAFS spectra ($k^3\chi(k)$, insets) for **6**. Experimental data is shown with dotted lines (•••), while fits are shown with solid lines (——). Fourier transformation range: $k = 2 – 14$ Å^{-1}. Fit parameters associated with the stated fit are shown in Table S6.

Table S7. Cartesian coordinates for the optimized structure of **5** (Figure S14). Gaussian 09, B3LYP/ 6-311G.

Fe	0.53600600	0.17770700	0.16325700
O	1.65930100	0.89762600	1.12723600
N	-1.06591400	0.41757500	1.52049600
C	-0.94730400	-0.72880400	2.52421900
H	-1.28997900	-0.38735100	3.50228500
H	-1.62115900	-1.52239400	2.20787800
C	0.47388600	-1.24262400	2.60644000
H	1.13558900	-0.48689900	3.01669800
H	0.51873900	-2.12534500	3.24923900
N	0.98703400	-1.58761400	1.22247700
C	2.49438000	-1.77774300	1.33052800
H	2.66841200	-2.68701600	1.91189700
H	2.87195900	-0.93150800	1.89639700
C	3.23847900	-1.86487700	0.00087000
H	2.92866600	-2.73350400	-0.58154800
H	4.28629400	-2.05651400	0.24846600
C	3.22297300	-0.59058700	-0.84473100
H	3.57363200	0.25264500	-0.25541100
H	3.89254800	-0.72001700	-1.69910300
N	1.85742800	-0.20955600	-1.40204700
C	1.98674300	1.08273700	-2.20524800
H	3.00278500	1.16617300	-2.59322000
H	1.32362100	1.00509300	-3.06325300
C	1.64176800	2.28635600	-1.35892400
H	2.36899000	2.42420200	-0.56601400
H	1.61977000	3.19169900	-1.97015500
N	0.29081600	2.08402700	-0.69696600
C	0.15219500	3.15497800	0.37479700
H	0.06736000	4.11921400	-0.13355700
H	1.07993000	3.14664600	0.93842700
C	-1.02086200	2.98361200	1.33816600
H	-1.97869400	3.06726500	0.81979400
H	-0.99943500	3.85069000	2.00439800
C	-0.97151700	1.75170000	2.24502800
H	-0.03314700	1.73391600	2.79363000
H	-1.79154500	1.79883600	2.96755900
C	-2.39256400	0.29128400	0.81538300
H	-2.74814700	1.27750900	0.52655400
H	-3.13365400	-0.12285200	1.49799800
C	-2.20598900	-0.55206500	-0.42967500
O	-0.99024700	-0.66905400	-0.86213800
N	-3.23108200	-1.11701100	-1.05631800
C	-4.64609600	-0.97226900	-0.63597400
H	-4.78120500	-0.13730100	0.04293000
H	-4.99197100	-1.88986900	-0.16050800
H	-5.25166300	-0.78784700	-1.52060300
C	-3.02039600	-1.94903700	-2.26487900
H	-1.96704500	-2.17294400	-2.37581000
H	-3.37827700	-1.41715200	-3.14608700
H	-3.58379900	-2.87386400	-2.15676000
C	0.35584500	-2.86934100	0.75417600
H	0.60314800	-3.67424900	1.44876200
H	0.72284400	-3.13367200	-0.22914400
H	-0.72131300	-2.77180600	0.69343500
C	1.40078400	-1.27681000	-2.36819000
H	2.12281200	-1.35426100	-3.18300100
H	0.42769400	-1.01406700	-2.76300500
H	1.32553100	-2.23721800	-1.87743700
C	-0.79733200	2.23871400	-1.72229000
H	-0.69405500	3.19948200	-2.22969000
H	-1.77084100	2.21194300	-1.24563700
H	-0.75090700	1.44007900	-2.45352800

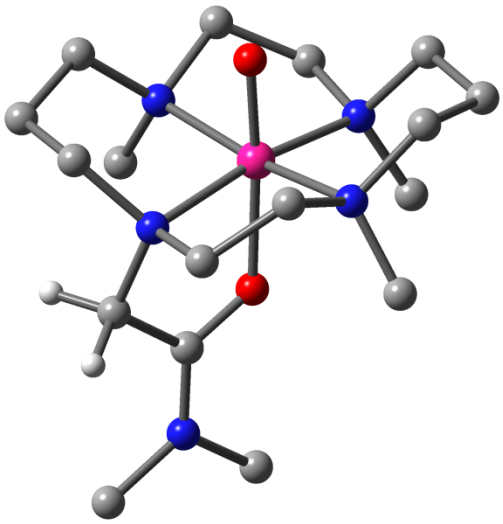

Figure S16. Geometry optimized structure of **5**, generated using Gaussian 09, B3LYP/ 6-311G. Atoms are colored according to: pink=iron, red=oxygen, blue=nitrogen, gray=carbon, white=hydrogen. Hydrogen atoms are omitted for clarity, except for the two hydrogens of the methylene linker.

Table S8. Cartesian coordinates for the optimized structure of **6** (shown in Figure S15). Gaussian 09, B3LYP/ 6-311G.

Fe	0.49439900	0.17020500	0.21672300				
O	1.59767000	0.86088100	1.25884500	H	-2.34676600	2.38543700	1.28081100
N	-1.01995600	-0.03652000	1.62484500	H	-1.56332000	3.23328300	2.59028500
C	-0.69974600	-1.28540700	2.45252000	C	-1.10454500	1.15945400	2.54289600
H	-0.99513200	-1.11781200	3.48986300	H	-0.15816100	1.22378100	3.07676300
H	-1.32231300	-2.08402400	2.06073700	H	-1.90072500	0.96015500	3.26745500
C	0.77070400	-1.63199600	2.37151200	C	-2.27473900	-0.23584400	0.87556400
H	1.36904900	-0.86988900	2.85979200	H	-3.19537300	-0.19169000	1.43318100
H	0.96492600	-2.59692100	2.84968800	C	-2.11127100	-0.66838400	-0.41260800
N	1.21791700	-1.67979900	0.92701400	O	-0.85451200	-0.62962700	-0.93193000
C	2.73190700	-1.71578400	0.92597100	N	-3.11446100	-1.14341300	-1.22448100
H	3.04151200	-2.68892000	1.32069100	C	-4.47832000	-1.25059700	-0.70627600
H	3.05379800	-0.94381300	1.61834100	H	-4.47883000	-1.73303400	0.27211400
C	3.40038100	-1.47425200	-0.42582900	H	-5.06806900	-1.86245400	-1.38504000
H	3.13272900	-2.24425000	-1.15047100	H	-4.96650900	-0.27379400	-0.61070000
H	4.47514400	-1.59883500	-0.26405100	C	-2.91715400	-1.32369800	-2.66423500
C	3.20709800	-0.07316600	-1.01044200	H	-1.85475900	-1.31934200	-2.87845000
H	3.47574800	0.67487200	-0.26882800	H	-3.40359400	-0.53161000	-3.24409800
H	3.86089100	0.04464300	-1.88121200	H	-3.33283600	-2.28233500	-2.97824300
N	1.79341500	0.23207300	-1.45658000	C	0.66692200	-2.90468800	0.25833500
C	1.72863800	1.65109000	-1.99981100	H	0.93697700	-3.79230900	0.83655800
H	2.71277500	1.94452700	-2.37149100	H	1.07616700	-3.00054100	-0.74021200
H	1.05454800	1.64577100	-2.85269800	H	-0.40898700	-2.83386700	0.16456300
C	1.25180000	2.62942600	-0.94660400	C	1.40858400	-0.69105900	-2.58090700
H	1.98297000	2.72328100	-0.15066300	H	2.10784500	-0.56408300	-3.41159600
H	1.08722600	3.61500600	-1.39239700	H	0.39908600	-0.46245400	-2.89373400
N	-0.02697100	2.13667800	-0.31292000	H	1.42393200	-1.72167600	-2.25496900
C	-0.28356600	2.97894900	0.91949200	C	-1.17182500	2.28047800	-1.27166900
H	-0.51016000	3.99597200	0.58286100	H	-1.27048900	3.32721900	-1.57066900
H	0.64819400	2.99765800	1.47781500	H	-2.08608600	1.95026100	-0.79354400
C	-1.40452300	2.47080100	1.82238300	H	-1.01272200	1.66134200	-2.14545400

Figure S17. Geometry optimized structure of **6**, generated using Gaussian 09, B3LYP/ 6-311G. Atoms are colored according to: pink=iron, red=oxygen, blue=nitrogen, gray=carbon, white=hydrogen. Hydrogen atoms are omitted for clarity, except for that which remains after deprotonation of the methylene linker of the pendant donor arm to form **6.**

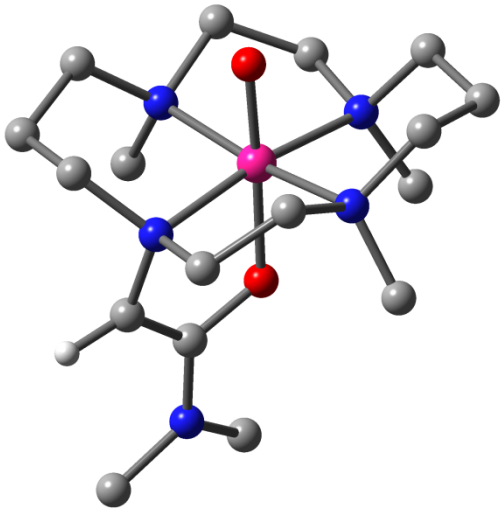

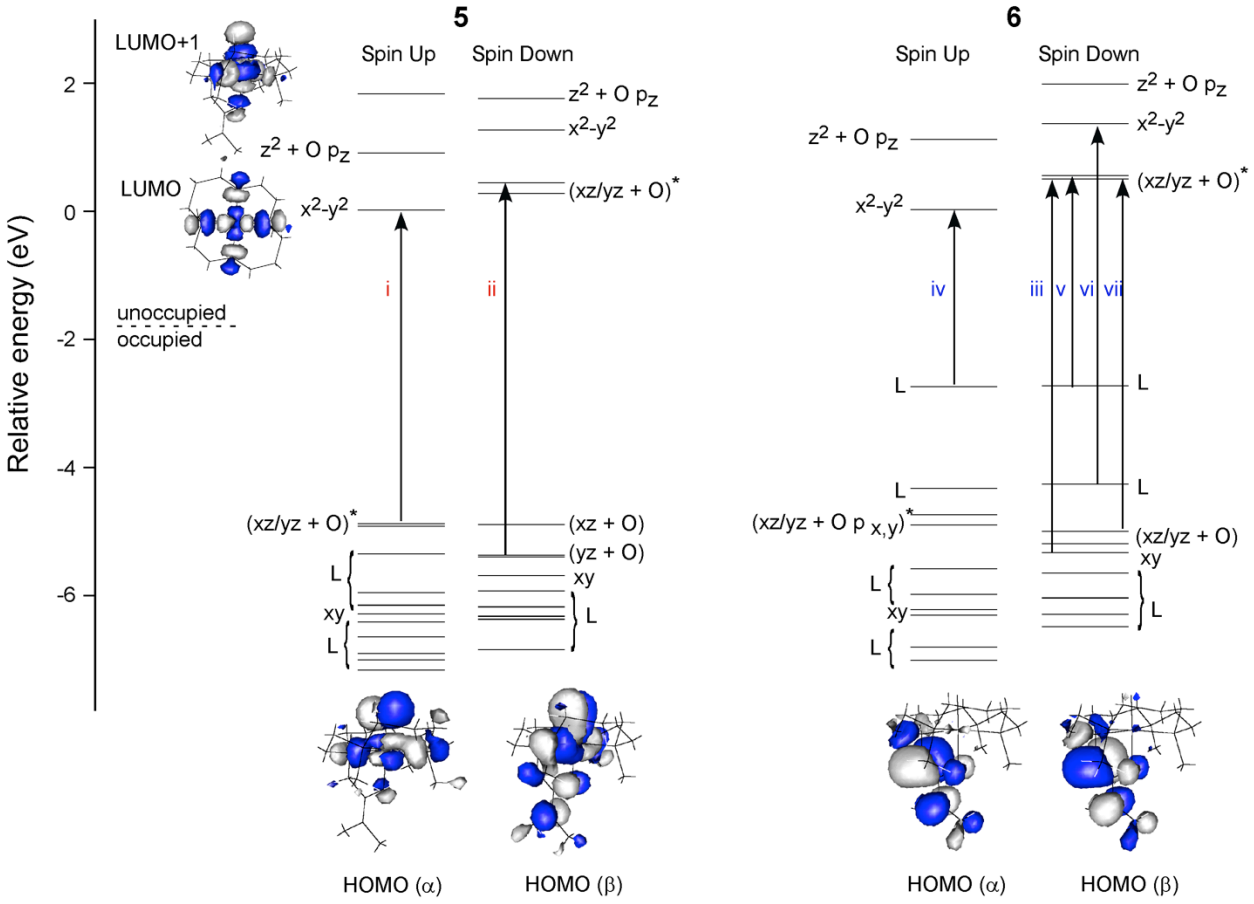

Figure S18. (Top) Relative energies and selected isosurface plots of the molecular orbitals of **5** and **6** generated using spin-unrestricted TD-DFT calculations. Arrows indicate electronic transitions that give rise to the experimentally observed optical features shown in Figure 11. (Bottom) Isosurface plots of the highest occupied molecular orbitals, where α indicates spin up and β indicates spin down.

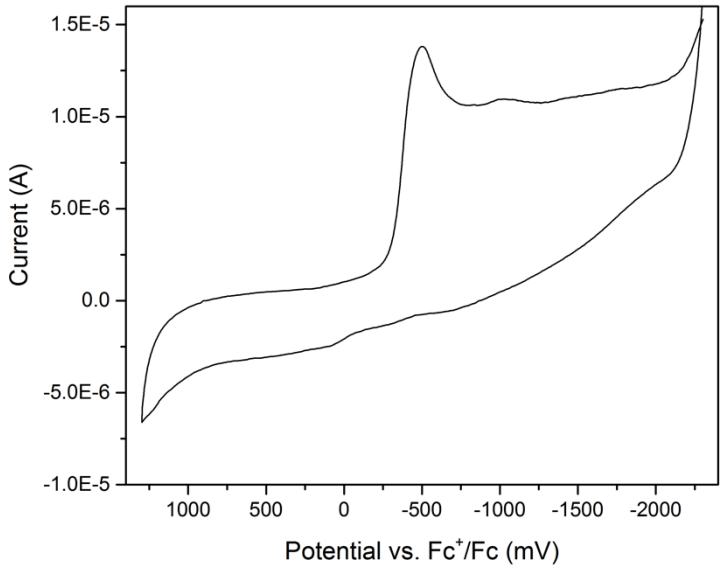

Figure S19. Cyclic voltammogram of **3**, recorded at room temperature in CH_3CN solution containing 0.1 M NBu_4PF_6 electrolyte at a scan rate of 100 mV s^{-1}. Potentials plotted versus the Fc^+/Fc couple.

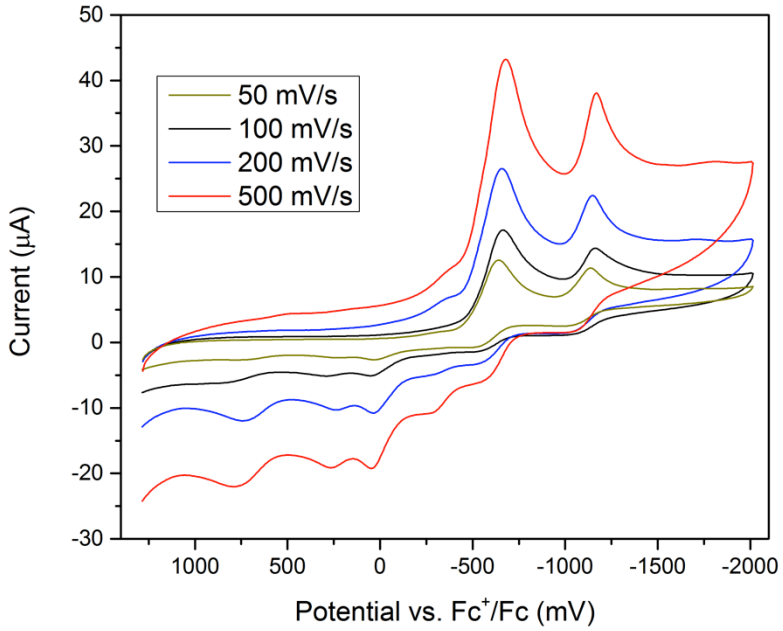

Figure S20. Cyclic voltammetric trace of **5** as a function of scan rate, recorded at room temperature in CH_3CN solution containing 0.1 M NBu_4PF_6 electrolyte. Potentials plotted versus the Fc^+/Fc couple.

References

1. H. Saltzman and J. G. Sharefkin, *Org. Synth.* , 1963, **43**, 60-61.
2. J. R. Hagadorn, L. Que and W. B. Tolman, *Inorg. Chem.*, 2000, **39**, 6086-6090.
3. C. Bucher, E. Duval, J.-M. Barbe, J.-N. Verpeaux, C. Amatore and R. Guilard, *C. R. l'Academie. Sci., Ser. IIC*, 2000, **3**, 211-222.
4. L. Toib, S. Dermaik, M. Michman and Y. Sasson, *Synlett*, 1995, 245-246.
5. R. H. Blessing, *Acta Crystallogr., Sect. A: Found. Crystallogr.* , 1995, **A51**, 33-38.
6. S. V6.45, Bruker Analytical X-Ray Systems, Madison, WI 2003.
7. S. V6.14, Bruker Analytical X-Ray Systems, Madison, WI 2000.
8. B. C. Schardt and C. L. Hill, *Inorg. Chem.*, 1983, **22**, 1563-1565.
9. G. N. George, Stanford Synchrotron Radiation Laboratory, Stanford Linear Accelerator Center, Stanford, CA, 2000.
10. R. C. Scarrow, M. G. Trimitsis, C. P. Buck, G. N. Grove, R. A. Cowling and M. J. Nelson, *Biochemistry* 1994, **33**, 15023-15035.
11. A. L. Ankudinov, B. Ravel, J. J. Rehr and S. D. Conradson, *Phys. Rev. B*, 1998, **58**, 7565-7576.
12. P. J. Riggs-Gelasco, T. L. Stemmler and J. E. Penner-Hahn, *Coord. Chem. Rev.*, 1995, **144**, 245-286.
13. G. W. T. M. J. Frisch, H. B. Schlegel, G. E. Scuseria, M. A. Robb, J. R. Cheeseman, G. Scalmani, V. Barone, B. Mennucci, G. A. Petersson, H. Nakatsuji, M. Caricato, X. Li, H. P. Hratchian, A. F. Izmaylov, J. Bloino, G. Zheng, J. L. Sonnenberg, M. Hada, M. Ehara, K. Toyota, R. Fukuda, J. Hasegawa, M. Ishida, T. Nakajima, Y. Honda, O. Kitao, H. Nakai, T. Vreven, J. A. Montgomery, Jr., J. E. Peralta, F. Ogliaro, M. Bearpark, J. J. Heyd, E. Brothers, K. N. Kudin, V. N. Staroverov, T. Keith, R. Kobayashi, J. Normand, K. Raghavachari, A. Rendell, J. C. Burant, S. S. Iyengar, J. Tomasi, M. Cossi, N. Rega, J. M. Millam, M. Klene, J. E. Knox, J. B. Cross, V. Bakken, C. Adamo, J. Jaramillo, R. Gomperts, R. E. Stratmann, O. Yazyev, A. J. Austin, R. Cammi, C. Pomelli, J. W. Ochterski, R. L. Martin, K. Morokuma, V. G. Zakrzewski, G. A. Voth, P. Salvador, J. J. Dannenberg, S. Dapprich, A. D. Daniels, O. Farkas, J. B. Foresman, J. V. Ortiz, J. Cioslowski, D. J. Fox, Gaussian, Inc., Wallingford CT, 2010.
14. F. Neese, *ORCA 2.6.35, an ab initio, density functional, and semiempirical program package*, Max-Planck-Institut für Bioanorganische Chemie, Mülheim an der Ruhr, Germany, 2008.
15. C. Adamo and V. Barone, *J. Chem. Phys.*, 1999, **110**, 6158-6170.
16. N. Godbout, D. R. Salahub, J. Andzelm and E. Wimmer, *Can. J. Chem.*, 1992, **70**, 560.
17. A. Schafer, H. Horn and R. Ahlrichs, *J. Chem. Phys.*, 1992, **97**, 2571-2577.
18. L. Laaksonen, *Journal of Molecular Graphics*, 1992, **10**, 33-34.